Enhanced Capacity and Rate Capability of Carbon Nanotube Based Anodes with Titanium Contacts for Lithium Ion Batteries

Roberta A. DiLeo, Anthony Castiglia, Matthew J. Ganter, Reginald E. Rogers, Cory D. Cress, Ryne P. Raffaelle, and Brian J. Landi*

Rochester Institute of Technology, 156 Lomb Memorial Drive, Rochester, New York 14623, National Renewable Energy Laboratory, Golden, Colorado, 84041, and U.S. Naval Research Laboratory, Washington D.C. 20375

ABSTRACT Carbon nanotubes are being considered for adoption in lithium ion batteries as both a current collector support for high-capacity active materials (replacing traditional metal foils) and as free-standing electrodes where they simultaneously store lithium ions. The necessity to establish good electrical contact to these novel electrode designs is critical for success. In this work, application of nickel and titanium as both separable and thin film electrical contacts to free-standing single-wall carbon nanotube (SWCNT) electrodes is shown to dramatically enhance both the reversible lithium ion capacity and rate capability in comparison with stainless steel. Scanning electron microscopy showed that evaporation of Ni and Ti can effectively coat the SWCNT bundles in a bulk electrode which is capable of providing an improved electrical contact. A thin film of titanium emerged as the preferred electrical contact promoting the highest capacity ever measured for a SWCNT free-standing electrode of 1250 mAh/g. In addition, the titanium contacting approach demonstrated a 5-fold improvement in lithium ion capacity at extraction rates greater than 1*C* for a high-energy density Ge—SWCNT electrode. The overall performance improvement with Ti contacts is attributed to a lower contact resistance, nanoscale "wetting" of SWCNT bundles to improve contact uniformity, and effective electron coupling between Ti and SWCNTs due to work function—energy level alignment. The experimental results provide the basis for a Ragone analysis (power *vs* energy parameters), whereby Ge—SWCNT—Ti anodes paired with a $LiFePO_4$ cathode can lead to a 60% improvement over conventional graphite anodes in both power and energy density for a complete battery.

KEYWORDS: lithium ion batteries · carbon nanotubes · free-standing anodes · germanium anodes · titanium contacts

Lithium ion (Li^+) battery technology is at the forefront of development to meet the growing electrical storage need presented by mobile electronics,[1] renewable energy development,[2] and electric (EV) and plug-in hybrid electric vehicles (PHEV).[2,3] Conventional Li^+ batteries can benefit from an increase in reversible capacity, cycle life, and charge−discharge rates, which come from modification of cell design and selection of novel active materials.[2] The cell designs are generally directed at either high-power (W/kg) or high-energy (Wh/kg) applications resulting in trade-offs between active materials (*e.g.*, cathode may be $LiNiCoAlO_2$ for high energy or $LiFePO_4$ for high power), composite thickness, and ratio of binder to conductive additives to minimize ohmic losses under high-power operation.[4] However, recent interest in a more balanced battery design regarding the power/energy ratio is motivated by the Department of Energy's requirement to make EVs and PHEVs a reality by overcoming range barriers.[3]

Recent efforts to identify new active materials and battery designs that are capable of high capacity over a range of charge/discharge rates have focused on utilizing various carbonaceous and inorganic nanomaterials.[2,5] The nanomaterial size allows for higher capacity at high currents because of the shorter diffusion parameters, as well as the ability to more readily accommodate expansion and contraction during lithiation because of the bond stretching, which leads toward more robust materials.[6,7] In particular, specific attention has been given to the potential of carbon nanotubes (CNTs) for lithium ion batteries,[8−22] due to their unique combination of structural and electronic properties. Reversible capacities exceeding a LiC_2 stoichiometry (>1116 mAh/g) are proposed for single-wall carbon nanotubes (SWCNTs),[23,24] representing a dramatic improvement over conventional graphite limits.[25] In addition to the remarkable intrinsic properties, a further impact is the ability to process CNTs into free-standing electrodes, which can dramatically enhance the lithium ion capacity in a full battery.[26−28]

The novelty in free-standing electrode design comes from the ability to maintain

*Address correspondence to brian.landi@rit.edu.

Received for review July 30, 2010 and accepted September 09, 2010.

Published online September 21, 2010.
10.1021/nn1018494

bifunctionality (*i.e.*, role as both the active material with high lithium ion capacity and sufficient electron transport to remove the inactive current collector) in a battery. The implication of using a free-standing electrode is that the entire mass contributes to the usable electrode capacity (Ah/mass of electrode). Another important advantage for free-standing CNT anodes is the ability to adjust the anode thickness to tailor the electrode-specific capacity and achieve the ideal number of electrodes within a given volume. Such a strategy is not feasible with conventional designs because there is a nonlinear decrease in usable electrode-specific capacity as the composite thickness is thinned due to the relative increase in copper foil mass percent.[29] Measurements to date for SWCNT anodes have reported reversible capacities from 400 to 600 mAh/g for purified materials.[10,27,30−32] Further increases in capacity have been achieved through alternative processing conditions, such as inclusion of defects and shortening of carbon nanotubes through ball-milling,[33] optimization of electrolyte,[27] and higher temperature testing.[28] In general, the benchmark lithium ion capacity for a free-standing CNT anode is 1000 mAh/g.[9,34]

CNT electrodes can also offer a lightweight, stable structure to support ultrahigh capacity active materials.[26−28] Such a strategy capitalizes on electrical transport from the CNT percolation network and relies upon the proper incorporation of higher capacity crystalline materials such as semiconductors,[33,35−40] namely tin (994 mAh/g), germanium (1600 mAh/g), and silicon (4000 mAh/g). Most recently, inclusion of silicon and germanium within free-standing semiconductor−SWCNT anodes yielded electrode-specific capacities exceeding 1000 mAh/g with nominal anode voltages at 0.4−0.5 V *vs* Li/Li^+.[41,42] Given such progress in terms of enhancing the electrode capacity, there is a parallel need to maximize the power density in free-standing electrodes such that improvements in battery design can be realized for both power and energy intensive applications. The power capability is directly related to the ability to make good electrical contact to the CNT electrode in the battery design.

Efforts to develop good electrical contact to CNTs have been an area of both experimental and theoretical study in recent years.[43−57] The prospect of coating CNTs with a thin film of metal to establish low contact resistance has been studied for a variety of applications including hydrogen storage,[58] field emission devices,[59,60] and in microelectronic devices to individual carbon nanotubes or thin networks.[52−54,61−65] The prevalence for certain metals to interact favorably with the CNT surface has been corroborated by electron microscopy studies that evaluated the "wettability" of several metals with the concluding trend of Ti > Ni > Pd > Fe > Al > Au in their ability to adhere and uniformly coat carbon nanotubes.[66−68] Titanium and nickel were both shown to deposit in a conformal coating on individual CNTs, as compared to other studied metals which deposit in discrete-like particles on the carbon nanotube surface.[66−68] In addition to experimental results, theoretical calculations show that titanium and nickel are highly favorable metals for CNT contacts based upon carbon nanotube side-wall distortion, wetting theories, and surface energies.[43−46,49,50,53,69] However, progress to implement this understanding to a bulk CNT electrode has been limited,[70−73] with most attention given to gold (which was proposed to have poor carbon nanotube−metal interaction due to limited wettability). Thus, it is critical to identify proper electrical contacts to CNT anodes for battery applications to minimize ohmic losses as well as assess electrochemical stability for cell design.

In the present study, a comparison between separable and thin film metal contacts for free-standing SWCNT anodes was performed for two prevalent metals used in lithium ion battery technology and also known to interact favorably with CNTs: Ni and Ti. The electrochemical capacity and rate capability have been measured for pure SWCNT and Ge−SWCNT electrodes with and without metal contacts to assess the effects on reversible capacity and rate capability. The experimental values served as parametric inputs to a recently developed battery model that calculates the energy and power densities for a flat plate prismatic battery design utilizing $LiFePO_4$ as the cathode. The overall results are used to propose a physical rationale for performance improvements in the battery anode from the unique SWCNT−metal interactions.

RESULTS AND DISCUSSION

The present study investigates the electrochemical capacity and rate capability of free-standing SWCNT electrodes with and without Ti and Ni contacts to assess their candidacy for improved electrical contacts for battery electrodes. Nickel and titanium were selected as potential electrical contacts on coin cells because of their favorable compatibility with carbon nanotubes and their accepted use in the battery community. Initial measurements used separable metal contacts deposited on the cathode side of the half cell to investigate the interaction with SWCNT electrodes.

Figure 1a is the first cycle charge/discharge for the SWCNT electrodes in contact with the Ni- and Ti-metalized coin cells at a constant current of 74 mA/g with respect to the SWCNT mass. The purified free-standing SWCNT electrode (blue, 1) exhibits a specific capacity of 550 mAh/g, which is consistent with previous work for similar materials.[10,15,26−28,31,32,34,74] Figure 1a illustrates that the use of Ni- and Ti-metalized coin cell cans provides a marked improvement in the reversible lithium ion capacity for SWCNT electrodes achieving 680 and 1050 mAh/g, respectively. Each of the SWCNT electrodes in Figure 1 has a Coulombic efficiency of 20%, which is independent of metal contacting. Such a

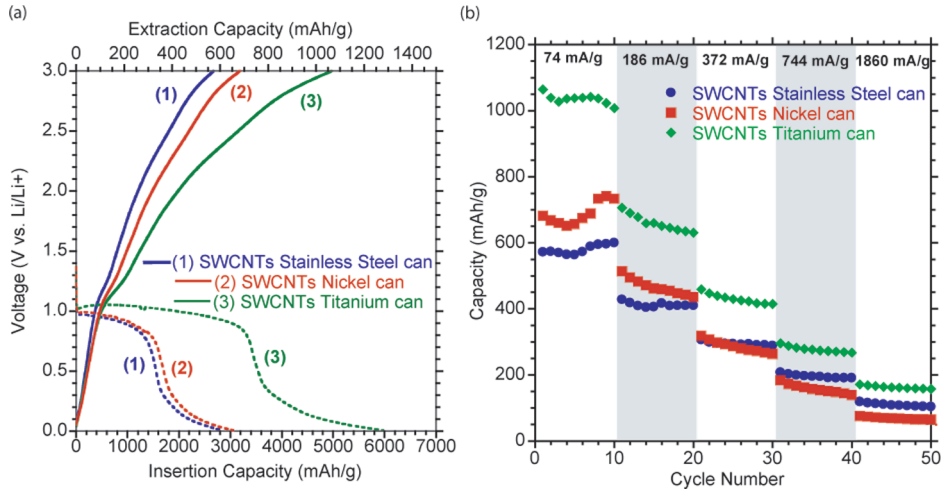

Figure 1. (a) First cycle insertion and extraction voltage profile for SWCNT electrodes on a stainless steel cell (blue, 1, ●) titanium-coated cell (green, 3, ◆), and a nickel-coated cell (red, 2, ■) at a current of 74 mA/g. (b) Cycling for the SWCNT electrodes on metalized coin cell cans at 74, 186, 372, 744, and 1860 mA/g.

loss can be addressed in full battery designs using prelithiation steps.[26−28] A reversible capacity of 1050 mAh/g exceeds the highest measured value to date for purified free-standing SWCNT electrodes and illustrates the opportunity to enhance lithium ion capacity with appropriate separable electrical contacts for these materials.

Figure 1b depicts the capacity for 50 cycles over five currents for each of the SWCNT electrodes measured in contact with the metalized coin cell cans. The nickel-metalized coin cell (red, ■) demonstrates an improvement in capacity over the stainless steel can at lower currents, but the improvement falls off as the rate of cycling is increased. The improvement in capacity with the use of a titanium-metalized coin cell (green, ◆) persists at higher currents, outperforming the conventional stainless steel and Ni-metalized coin cell cans. It is important to note that the reversible capacity of the SWCNT electrodes with Ti-metalized cans is stable over the number of cycles measured. Such an improvement in electrochemical performance observed through the use of titanium on the coin cell can may be attributed to the enhanced ohmic contact from reduced contact resistance at the junction with the SWCNT electrode.[48]

The measured improvements in reversible capacity for purified free-standing SWCNT electrodes with nickel and titanium separable contacts, as well as the known wettability of these metals onto the SWCNT surface,[51,68] warranted an investigation of direct deposition of the metals. The metals were evaporated onto SWCNT electrodes and are designated as SWCNT−Ni and SWCNT−Ti, respectively, to represent the [active material]−[thin film electrical contact]. Figure 2a shows an interface (top-down) between the high-purity SWCNT morphology and the 100 nm Ni coating on the

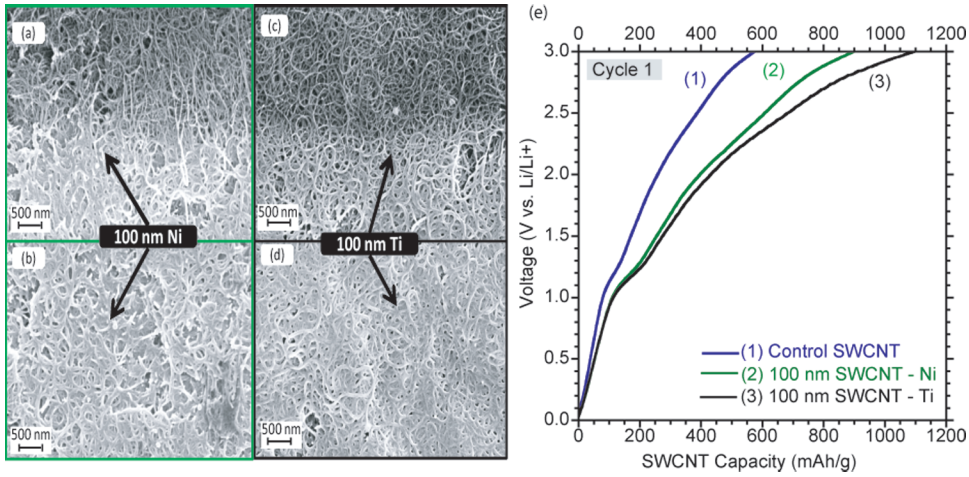

Figure 2. Scanning electron micrographs at 20 000× magnification of (a) the interface between coated and uncoated carbon nanotubes for 100 nm SWCNT−Ni electrode, and (c) the 100 nm SWCNT−Ti electrode. The uniform bundle coating is shown for the (b) 100 nm SWCNT−Ni electrode, and the (d) 100 nm SWCNT−Ti electrode. (e) First cycle extraction for a SWCNT electrode (blue, 1), the 100 nm SWCNT−Ni electrode (green, 2), and the 100 nm SWCNT−Ti electrode (black, 3) at a current of 74 mA/g with a standard electrolyte of 1 M $LiPF_6$EC/PC/DEC. The capacity is a function of SWCNT mass only.

SWCNTs, and Figure 2b shows an area completely coated with 100 nm of Ni. With a thickness of 100 nm, there is uniform metal coating on the SWCNT bundles, but the carbon nanotube morphology is still visible. Similar to the nickel deposition, the SEM images in Figure 2c,d show that the 100 nm titanium evaporation leads to a conformal coating of titanium over the SWCNT bundles in the electrode, as well.

Electrochemical half-cell testing was performed for the 100 nm SWCNT−Ni and SWCNT−Ti electrodes at five charge/discharge currents to investigate the effect on bundle coating within the bulk electrode. Figure 2e shows the first cycle extraction of the control SWCNT electrode (blue, 1), the 100 nm SWCNT−Ni electrode (green, 2), and the 100 nm SWCNT−Ti electrode (black, 3) at a constant current of 74 mA/g. The SWCNT−Ni electrode exhibits an increase in capacity for the first cycle of 880 mAh/g for the active SWCNT mass compared to the control SWCNT electrode of 550 mAh/g. The 100 nm SWCNT−Ti electrode shows an additional increase in reversible capacity up to 1100 mAh/g. Each of the SWCNT electrodes showed a comparable Coulombic efficiency regardless of deposited metal contact. It is of importance to note that there is no evidence to suggest the improvements in storage capacity are coming from lithium insertion into Ti or TiO_x, which would occur around 1.5−1.7 V,[75,76] but rather from enhanced storage within the SWCNTs.

Initial electrochemical characterization indicated titanium outperforms nickel, giving rise to the investigation of a thicker titanium layer. A 500 nm thick titanium layer, shown in Figure 3a,b, was deposited on the SWCNTs to determine if creating a thin film contact with the SWCNT bundles and a complete filling of nanopores within the SWCNT electrode would further increase the active material capacity. Figure 3c illustrates the first cycle extraction capacity for the electrode series scaled with respect to the entire electrode mass. The performance of the 500 nm SWCNT−Ti electrode (red, 3) is close to that of the 100 nm SWCNT−Ti electrode (black, 4), with specific electrode capacities of 925 and 1000 mAh/g, respectively. The lack of any improvement with the thicker titanium film suggests that a 100 nm film is sufficient to improve electrochemical performance of the SWCNT electrodes; however, it is possible that slight modifications in the titanium thickness of 100 up to 500 nm may provide an even higher lithium ion storage capacity within the SWCNT active material. Even with the inclusion of the inactive metal contact mass, the metalized SWCNT electrode still significantly outperforms the control SWCNT electrode in specific capacity, 750 mAh/g for the SWCNT−Ni electrode, 925 and 1000 mAh/g for the 500 and 100 nm SWCNT−Ti, respectively.

There is a significant increase in capacity over the first 10 cycles in the SWCNT−Ti samples, which is attributed to an increase in the number of accessible lithium ion storage sites as the half-cell is cycled. Figure 3d shows the extraction curve of the tenth cycle for the to-

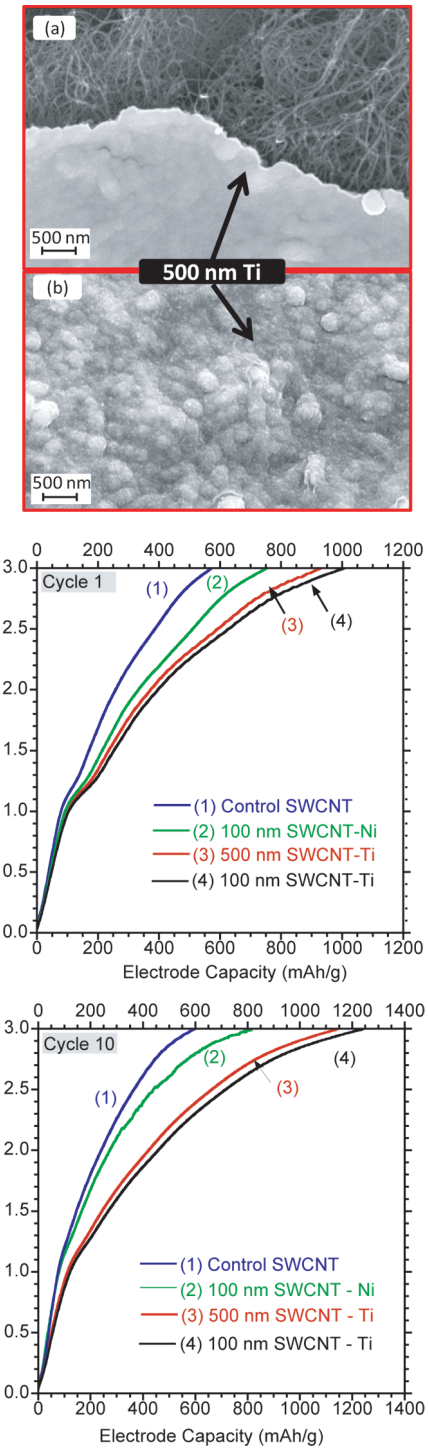

Figure 3. Scanning electron micrographs at 20 000× magnification of (a) the interface between coated and uncoated carbon nanotubes for the 500 nm SWCNT−Ti electrode and (b) the SWCNT−Ti completely coated with titanium; (b) first cycle extraction for the total free-standing electrode mass for a SWCNT electrode (blue, 1), the SWCNT−Ni electrode (green, 2), and the SWCNT−Ti electrodes at thicknesses of 100 nm (black, 4) and 500 nm (red, 3) at a current of 74 mA/g with a standard electrolyte of 1 M $LiPF_6$ EC/PC/DEC; and (c) the extraction for cycle 10 of the total free-standing electrode mass, at 74 mA/g.

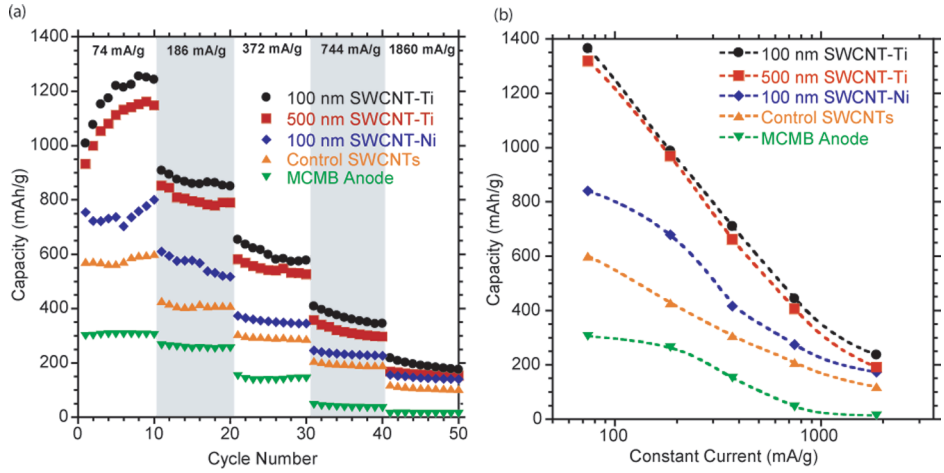

Figure 4. (a) Lithium ion capacity as a function of cycle number for the SWCNT electrode (orange,▲), the SWCNT−Ni (blue,◆), the SWCNT−Ti electrodes (100 nm, black, ●; 500 nm, red, ■), and a MCMB anode (green,▼) for five charge/discharge currents (74, 186, 372, 744, and 1860 mA/g) at 10 cycles for each current. (b) Maximum lithium ion capacity for each of the electrodes at a constant current with dashed trend lines for figure clarity.

tal electrode mass for all the electrodes, indicating the increased capacity after 10 cycles with values as high as 1250 mAh/g for the 100 nm SWCNT−Ti electrode. The enhanced electrical contact by the titanium with the SWCNTs is shown to increase capacity over the first few cycles and would be included during a protocol for conditioning in a full battery. The additional capacity may be attributed to lithium ion insertion around inner carbon nanotubes within the close-packed bundles, making a larger percentage of available SWCNTs active for charge transport. Overall, the capacity for a SWCNT−Ti electrode represents the highest measured value to date for a free-standing SWCNT electrode.

Figure 4a shows the full electrode capacity for the SWCNT, SWCNT−Ni, SWCNT−Ti, and MCMB anodes as a function of cycle number with 10 cycles shown for each current rate, determined from the active material mass (74, 186, 372, 744, 1860 mA/g). Each of the electrodes decreases in capacity as the current increases; however, the SWCNT−Ti electrode maintains an increase in capacity by more than 90% at the higher current rates. For comparison, a standard mesocarbon microbead (MCMB) anode was prepared and tested under the same half-cell and constant current conditions. The MCMB anode exhibits capacity reduction at higher currents, as well, with capacity reducing to less than 10% of the initial capacity at a current of 1860 mA/g. The significant improvement in rate capability for the SWCNT−Ti electrode over the MCMB anode is evidenced by a more than doubling in capacity even at similar *C* rates. Figure 4b shows that for a comparable 1*C* rate, the SWCNT−Ti electrode has a capacity of 350 mAh/g, which outperforms the state-of-the-art MCMB anode with a capacity of 200 mAh/g.

The significant improvement in electrochemical performance of laser vaporization synthesized SWCNTs with the use of titanium as a metal contact is clearly demonstrated in this study. A similar effect in increased capacity has also been measured with other SWCNT materials, namely, HiPCO synthesized CNTs (Unidym) and commercially available CNTs (Nanocomp Technologies, Inc.). The results illustrate that the choice of metal is critical to improve electrochemical performance as well as the deposited thickness, as it can influence the overall free-standing electrode specific capacity. The present results show that a 500 nm thick Ti contact does not improve the electrode specific capacity nor rate capability over a 100 nm thick film. Thus, the least amount of Ti necessary to improve the electrode performance is critical from an energy density standpoint since the titanium is an inactive material in the anode. An optimal Ti contact layer thickness will be directly related to the morphology of the free-standing SWCNT electrode, including the diameter and length distribution of the CNTs along with the degree of carbon nanotube bundling which influences the electrode porosity. In addition, the use of titanium over a traditional copper substrate maintains the opportunity for a battery capable of deep discharge to improve battery storage and performance after extended periods of inactivity.[77]

The measured improvement in capacity for SWCNT−Ti electrode rate capability could lead to development of a battery that performs in both high-power and high-energy applications. To further advance this concept, a thin film of titanium (100 nm) was used on the backside of a Ge−SWCNT electrode in a design that was previously measured to increase the anode energy density by a factor of 3 compared to conventional MCMB anodes.[42] Electron-beam evaporation was used for the deposition of titanium and germanium to ensure accurate thickness control monitoring. Figure 5a shows the first cycle extraction electrode capacity for a Ge−SWCNT electrode (700 mAh/g) and a Ge−SWCNT−Ti electrode (1200 mAh/g) where the titanium side is in contact with the coin cell can. The Ge−SWCNT−Ti electrode maintains the same favor-

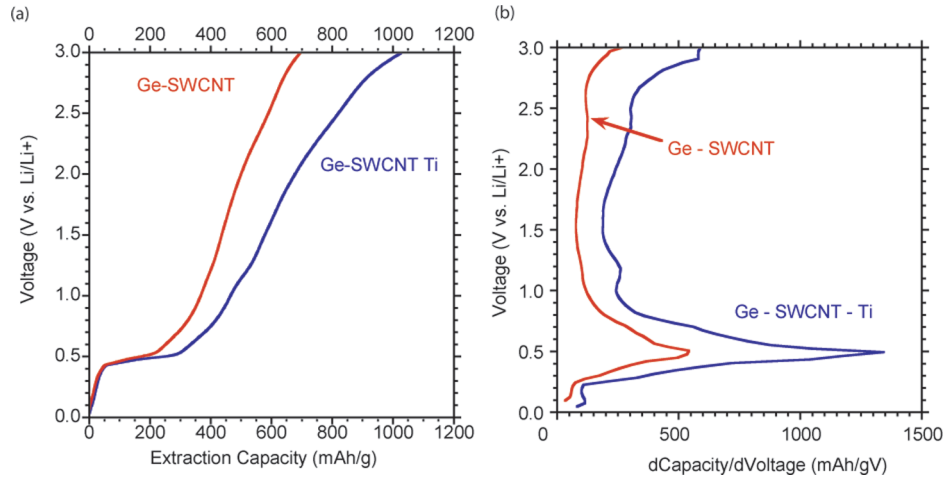

Figure 5. (a) First cycle extraction for a Ge−SWCNT electrode (red) and a Ge−SWCNT electrode with a Ti thin film (blue) at a current of 74 mA/g with a standard electrolyte of 1 M $LiPF_6$ EC/PC/DEC. (b) Differential change in capacity (d*C*/d*V*) as a function of voltage from 5 mV to 3 V; the axes are rotated to emphasize the correlation with the extraction voltage profile in (a).

able voltage profile as a Ge−SWCNT electrode but with an enhancement which improves the effective energy density of the anode when paired with a cathode in a full battery.[42] Figure 5b shows the differential change in capacity as a function of voltage for both the Ge−SWCNT and Ge−SWCNT−Ti electrodes. The results clearly illustrate the relative improvement in reversible Li^+ capacity for both Ge (predominant contribution between <1 V) and SWCNTs (>1 V) with the deposition of Ti contacts. The additional contribution from the SWCNTs below 1.5 V with the use of titanium is evidenced by the additional peak at ~1.2 V present in the Ge−SWCNT−Ti half-cell data.

Rate capabilities of the Ge−SWCNT and Ge−SWCNT−Ti electrodes were examined under five currents (74, 186, 372, 744, 1860 mA/g) at 10 cycles each, and the capacities are shown in Figure 6a. Similar to the performance of the SWCNT−Ti electrodes depicted in Figure 4, the improvement in capacity with the use of titanium for the Ge−SWCNT electrodes persists at higher rates. Figure 6b shows that for a comparable 1*C* rate (using the dashed lines as a guide) the Ge−SWCNT electrode has a capacity of 200 mAh/g, whereas the Ge−SWCNT−Ti electrode would have a capacity of approximately 550 mAh/g. Calculations also showed that the ratio of the storage capacity within the germanium, below 1 V, and within the SWCNTs, above 1 V, persists at the higher *C* rates, suggesting the capacity of the germanium is not completely reduced at higher currents. Such results for the Ge−SWCNT−Ti electrode dramatically exceed the conventional MCMB values from Figure 4 and represent a benchmark rate capability for free-standing anodes. Furthermore, the electrochemical results herein demonstrate that the electrical conductivity of the SWCNT−Ti electrode is a sufficient current collector (as a replacement for copper foil) to support the Ge-active material in the anode for applications with modest rate demands.

The experimental results for the Ge−SWCNT−Ti electrodes show that a dramatic improvement in

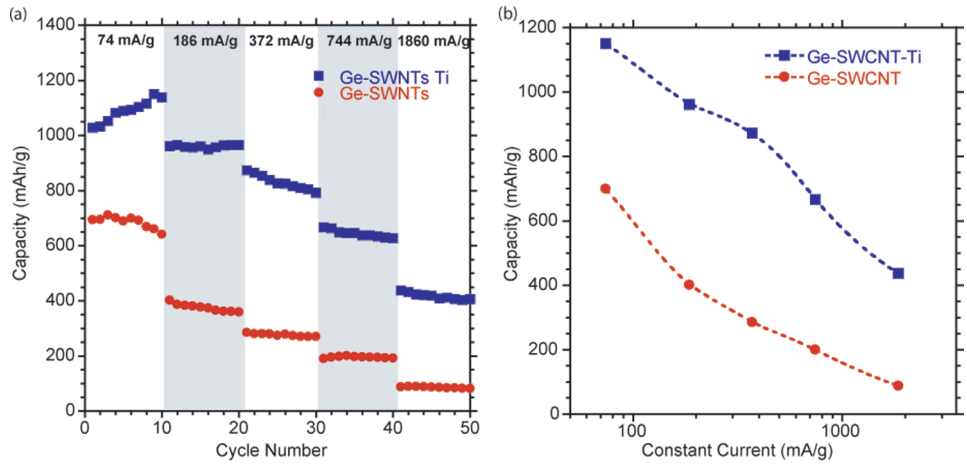

Figure 6. (a) Lithium ion capacity as a function of cycle number for the Ge−SWCNT electrodes without (red, ●) and with (blue, ■) titanium for five charge/discharge currents (74, 186, 372, 744, 1860 mA/g) at 10 cycles for each current. (b) Maximum lithium ion capacity for each of the electrodes at a constant current with dashed trend lines for figure clarity.

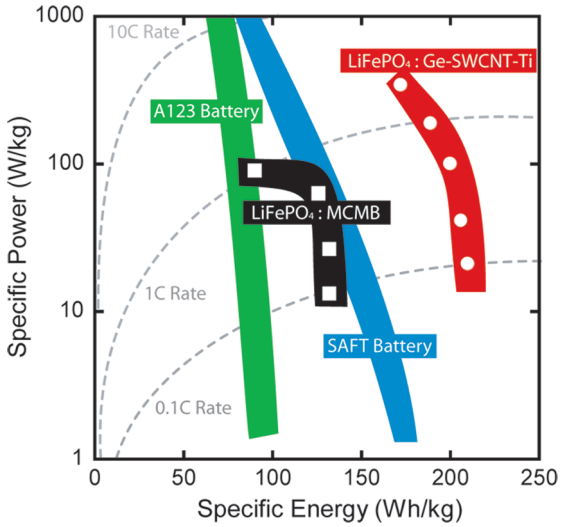

Figure 7. Ragone plot with the calculations from the numerical model for the MCMB anode (black, ■) and a Ge−SWCNT−Ti anode (red, ●) paired with a $LiFePO_4$ cathode. The green and blue bands illustrate the typical range of values for two commercial lithium ion battery designs from A123 and Saft, respectively. Dashed lines for 0.1, 1, and 10*C* rates are shown in gray.

lithium ion capacity can be achieved at *C* rates >1*C*, which could improve both the power and energy density in a full battery. Incorporation of the measured capacity values into a battery model, recently described, can provide a theoretical estimate on the relative improvement in the energy density of a full battery.[29,42] The model calculations consider the direct replacement of MCMB anodes on traditional copper current collectors with the free-standing Ge−SWCNT−Ti anodes. The algorithm pairs the anode with a $LiFePO_4$ cathode and determines the theoretical energy density improvements for a given cell composition based on the measured free-standing anode capacities. The control anode is similar to the one highlighted in Figure 4 for an MCMB composite, and the cathode model assumptions are equivalent to previously reported parameters.[29,42] Selection of $LiFePO_4$ as a suitable cathode match for the present design is based on the excellent rate capability for this cathode that leads to minimal capacity fade at modest *C* rates based upon previous work.[78]

Figure 7 highlights the outcome of the model calculations in the Ragone plot for the Ge−SWCNT−Ti:$LiFePO_4$ batteries based upon the measured capacity and rate studies from Figure 6. Thus, the specific energy density for a full battery with the Ge−SWCNT−Ti anodes paired with $LiFePO_4$ can become as high as 210 Wh/kg at low rate and exceed 175 Wh/kg at a 2*C* rate. This is a dramatic improvement over calculated energy densities for the MCMB anode paired with $LiFePO_4$, representing a 60% increase in energy density over the range of *C* rates when using a Ge−SWCNT−Ti free-standing anode. In addition, Figure 7 illustrates the performance values by the shaded bands for commercial lithium ion batteries from A123 systems (experimental data on their 18 650 cells containing the nanophosphate chemistry) and SAFT's reported data for their VLE technology.[79] Although not as high over the range of *C* rates, the SWCNT−Ti anode would exceed the MCMB−$LiFePO_4$ energy density (132 Wh/kg) by ~10%, even with the much lower average cell voltage (*i.e.*, 2 V). The proposed improvements in battery energy and power density with a Ge−SWCNT−Ti:$LiFePO_4$ design is clearly evident. It is interesting to note that the $LiFePO_4$ cathode, which is desirable for today's technologies due to the inherent safety, generally produces a lower energy density battery than its peer chemistries[80] but could achieve >200 Wh/kg with a Ge−SWCNT−Ti free-standing anode.

The collective results in the present study demonstrate a dramatic improvement in lithium ion capacity and rate capability for SWCNT electrodes with the use of Ni and Ti contacts. The improvements have been observed with both separable and thin film contacts with Ni illustrating modest increases and Ti contacts promoting dramatic increases in both capacity and rate capability. No additional improvement has been observed when contacting both the SWCNT electrode and the coin cell can in concert. Therefore, the overall enhancement is proposed to be governed by several factors including the following, as discussed in more detail below: (1) reduction of contact resistance at the electrode interface with metals, (2) SWCNT bundle coating by thin film deposition leading to a more uniform electrical contact at the nanoscale, and (3) energy level matching that promotes electron coupling to certain SWCNT chiralities.

The use of a metal, in general, has been reported to lower the contact resistance for CNT electrodes, which would allow for better charge transfer at the electrode−can interface.[43,48] In addition, if a metal can be deposited and "wet" the carbon nanotube surface, this will lead to a uniform coating on the SWCNT bundles which enhances the contact. If enough metal is deposited, it can ultimately fill the void space in the bulk carbon nanotube electrode and create a uniform thin film contact.[51,53,68] However, a complete thin film across the electrode does not improve the anode performance, which the 500 nm titanium layer demonstrated. Thus, a trade-off between the amount of inactive metal mass and the degree of coating on the SWCNT bundles will lead to the optimal SWCNT electrode capacity.

The wettability factor of these metals is heavily influenced by the interfacial energy and diffusion barriers, which are low and high, respectively, for titanium and nickel giving rise to the uniform coating.[46] In particular, titanium is reported to have higher binding energies to carbon nanotubes and a propensity to form conductive carbide bonds because of the 3d and 4d orbital vacancies, as compared to other metals.[46,50,68,81] An additional factor is proper alignment of the metal work function with the discrete-like energy states in SWCNTs for effective electron coupling.[82]

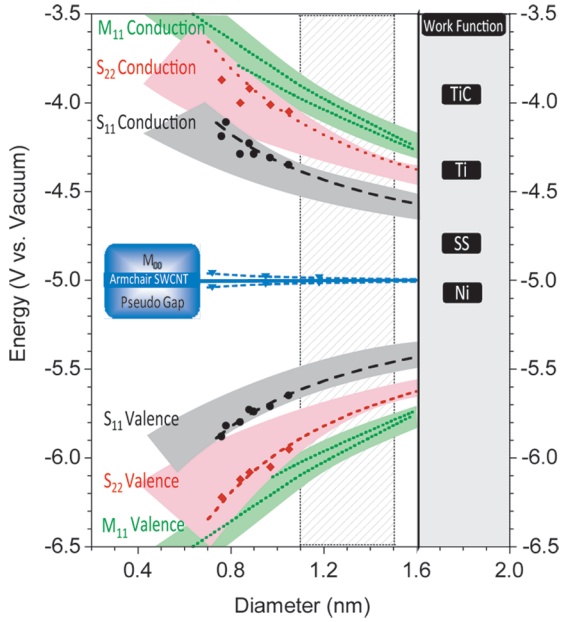

Figure 8. Schematic for the energy levels of semiconducting and metallic SWCNTs and metal work functions. Data points of semiconducting SWCNT first (black, ●) and second (red, ◆) conduction and valence states are from ref 89, and the curve fits, in corresponding color, are from ref 90. The metallic SWCNT conduction and valence trend lines (green) and bands (light green) and the semiconducting bands (gray and pink) are from a revised Kataura plot.[87] The work function of an isolated armchair nanotube (blue line) is from ref 85. The metallic SWCNT pseudogap data points and trend line (blue, ▼) are from STM measurements.[86] The Ti and Ni work function values were obtained from the CRC Handbook of Chemistry and Physics. The value for stainless steel is from ref 84 and TiC from ref 92. The hatched band extending from 1.1 to 1.5 nm depicts the diameter range of SWCNTs used for this work.

The schematic in Figure 8 depicts an energy level diagram for the various materials under investigation in this work. The work function values for the metals appear to the right,[83,84] while the left side of the figure shows both experimental and theoretical conduction and valence states for metallic and semiconducting SWCNTs. The work function for the only truly metallic SWCNT, an isolated armchair, is given as a solid blue line at 5.0 eV, which lies close to the middle of the band gap of the semiconducting carbon nanotubes.[85] The symmetric dashed lines (blue) running parallel to the metallic SWCNT work function are trend lines for the pseudogap values, from 20 to 100 meV, that are present for chiral and bundled "metallic" carbon nanotubes.[86] The blue data points are from experimentally measured values and fitted by the blue dashed line following the equation

$$E_{\text{m pseudogap}} = 3\gamma_o a_{cc}^2/16R^2 \quad (1)$$

where $\gamma_0 = 2.60$ eV, the tight-binding transfer matrix element, $a_{cc} = 0.142$ nm, the carbon−carbon bond distance, and R is the carbon nanotube radius.[86] The metallic (M_{11}) conduction and valence states are noted by the green shaded band from work based upon energy transitions in carbon nanotubes.[87] The dark green trend lines in these metallic transition bands arise from the trigonal warping effect resulting in "high" and "low" energy transitions for non-armchair carbon nanotubes.[87,88] The data points for the first and second conduction and valence states of semiconducting carbon nanotubes (S_{11} and S_{22}) come from experimental work with SWCNTs.[89] The dashed trend lines passing through the data points are consistent with these values based upon eq 2, where d_t is the carbon nanotube diameter, and was extrapolated to 1.6 nm diameter carbon nanotubes for the figure:[90]

$$E_{s\,\text{gap}} = (0.34\ \text{eV}/d_t) + (1.11\ \text{eV}/(d_t + 0.11)) \quad (2)$$

The corresponding shaded color regions of the semiconducting states also are based upon the SWCNT electronic transitions to reflect the range of possible values for a distribution of carbon nanotubes.[87] The diameter range of SWCNTs used in this work, 1.1−1.5 nm, is shown in the hatched region.

The first conduction state for the semiconducting carbon nanotubes (gray) lies in the range of 4.0−4.4 eV, which favorably aligns with the work function of titanium (4.33 eV), contributing to the improved performance demonstrated by titanium.[50,53,68,82,89] The alignment of nickel's work function (5.15 eV) with that of metallic carbon nanotubes (blue) could be favorable for electron transport at the metal−carbon nanotube interface and may explain the minor improvements with its use. However, the work function value of nickel less favorably aligns with the semiconducting carbon nanotube transition energy levels (gray and red) as compared to titanium. In addition, the work function for titanium carbide favorably aligns with the second excited state of semiconducting carbon nanotubes (red) used in this work (1.1−1.5 nm), again demonstrating the potential for an overlap in energy levels creating favorable electron transfer at the metal−carbon nanotube interface. While titanium and nickel both exhibit suitable characteristics, particularly during metal deposition, titanium emerges as the better contact metal in the electrochemical performance and is attributed to the combination of factors discussed.

The enhanced electrochemical performance for the Ge−SWCNT−Ti electrode, as illustrated in Figure 6, supports the mechanism for an improved charge transfer during the lithium ion extraction with a titanium contact. The Ge−SWCNT−Ti electrode design can foster a direct electron pathway between the Ti contact and the Ge active layer since the SWCNT electrode thickness is sufficient for a robust percolation network of SWCNT bundles. The use of a thin metal film (*e.g.*, titanium) that wets the backside of the Ge−SWCNT electrode can increase the number of conductive points of contact to the coin cell can. However, this alone showed limited improvement with a capable wetting metal such as nickel, and it was clearly evident that the SWCNT−Ti pairing is critical to enhanced capacity. Therefore, the

prospect that titanium's work function match to the conduction states for both semiconducting and metallic species is sufficient to promote electron transport through all chiralities in the SWCNT layer can explain the demonstrated improvements in Ge−SWCNT anode capacity and rate capability.

CONCLUSIONS

The use of Ni and Ti contacts to increase both the reversible lithium ion capacity and rate capability in free-standing SWCNT electrodes has been demonstrated. Both nickel- and titanium-coated coin cells were observed to increase capacity in SWCNT electrodes to over 650 and 1000 mAh/g, respectively. Further investigation showed a larger increase in reversible lithium ion capacity through direct deposition of metal on the SWCNT electrodes with capacities reaching the highest ever reported at 1250 mAh/g for the SWCNT−Ti electrodes. The approach was extended to a high-energy density Ge−SWCNT−Ti electrode, which demonstrated an increase in electrode capacity by more than 60% over the Ge−SWCNT electrode. The increase in capacity for this electrode results from both Ge and SWCNT contributions, over a series of *C* rates, offering the potential as both a high-energy and high-power density anode. The measured capacity and rate studies for the Ge-SWCNT-Ti electrodes were utilized in an empirical model to calculate the projected performance when coupled with a $LiFePO_4$ cathode in a full battery design. The calculations show the potential for a $LiFePO_4$ based battery with an energy density exceeding 175 Wh/kg up to a 2*C* rate, which represents a transformative development for this cathode chemistry without significant compromise in rate capability. The dramatic improvement with titanium is attributed to enhanced electrical contacting from the titanium−carbon nanotube interaction which fosters a reduced contact resistance from the conformal coating on the SWCNT bundles with the metal. A further implication of the titanium contacting results is that certain chiral SWCNT species (most likely semiconducting) may become more active to lithium storage when in contact with the titanium due to the proper work function alignment with the conduction states compared to nickel and stainless steel. Overall, this work advances the fundamental understanding of metal contacting with SWCNTs while demonstrating unprecedented lithium ion capacities for free-standing SWCNT anodes that can lead to a novel battery capable of both high-power and high-energy density.

METHODS

SWCNT Electrode Fabrication and Physical Characterization. Single-walled carbon nanotubes were synthesized through a laser vaporization process described previously.[91] In short, a nickel- and cobalt-doped graphite target was vaporized by a Nd:YAG laser under synthesis conditions of 200 sccm argon gas flow at 760 Torr and 1150 °C. The metal in the as-produced SWCNT material was removed through an acid reflux and filtered onto a PTFE filter to form a SWCNT paper. The SWCNT electrode was purified and acid removed by a thermal oxidation step to an equivalent level of 100% carbonaceous purity based upon previous reference materials for laser-synthesized materials resulting in electrode thicknesses of ~10 μm.[26,91] The carbon nanotube synthesis and purification methods used in this work resulted in a distribution of carbon nanotube properties, whereby both metallic and semiconducting SWCNTs are present with a distribution of chiralities and diameters over a range of 1.1−1.5 nm.[27]

Metal−SWCNT Electrode Fabrication. Nickel and titanium were deposited on the cathode side of 2032 stainless steel coin cell cans (Pred Materials International, Inc.), the SWCNT electrodes, and the Ge−SWCNT electrodes through thermal and electron-beam evaporation, respectively. The thickness of the metal deposited (*i.e.*, 100 or 500 nm) was based upon the effective thickness as measured using a quartz crystal oscillator. Germanium was deposited onto the SWCNT electrode through electron-beam evaporation for an effective thickness of 750 nm at a base pressure of 10^{-6} Torr. Scanning electron microscopy was performed using a LEO EVO 50 microscope (Zeiss) at a voltage of 10 keV.

Electrochemical Testing. Electrochemical testing of the electrodes was performed using 2032 coin cells prepared in an inert environment glovebox. A control anode composed of commercial MCMB active materials (Osaka Gas), polyvinylidene fluoride (Kynar), and a conductive carbon additive (Super P) was prepared using a composite coating ratio of 90:2:8 on copper foil (Fukuda Metal Foil & Powder Co., Japan). Half-cell testing consisted of SWCNT and SWCNT−Ti electrodes opposite lithium foil (Sigma Aldrich) with an electrolyte-soaked Celgard 2325 separator between. The electrolyte was a 1 M $LiPF_6$ (Sigma Aldrich) solution in a solvent mixture (1:1:2) of ethylene carbonate (EC), propylene carbonate (PC), and diethyl carbonate (DEC) (each purchased separately from Novolyte Technologies, Inc.). Galvanostatic cycling was performed with an Arbin Instruments BT-2000 at 28 °C from 3 V to 5 mV (V *vs* Li/Li^+). Five constant currents were applied for half-cell testing: 74 (equivalent of *C*/5 for LiC_6, where *C*/*t* is the *C* rate representing the complete charge (discharge) in *t* hours), 186, 372, 744, and 1860 mA/g.

Acknowledgment. The authors acknowledge financial support from the U.S. Government and Lockheed Martin. R.A.D. acknowledges graduate student funding from a GAANN fellowship through the RIT Microsystems Engineering PhD program. C.D.C. acknowledges financial support from the NRL Karles Distinguished Scholar Fellowship Program. The authors would like to thank Dr. Sean Rommel and David Pawlik for their assistance with the use of the LEO EVO 50 microscope, Tom Mastrangelo for his experimental assistance with the SWCNTs, and Jack Alvarenga and Chris Schauerman for their helpful discussions regarding this work.

REFERENCES AND NOTES

1. Endo, M.; Kim, C.; Nishimura, K.; Fujino, T.; Miyashita, K. Recent Development of Carbon Materials for Li Ion Batteries. *Carbon* **2000**, *38*, 183–197.
2. Daniel, C. Materials and Processing for Lithium-Ion Batteries. *J. Met., Mater. Miner.* **2008**, *60*, 43–48.
3. Howell, D. *Progress Report for Energy Storage Research and Development*; U.S. Department of Energy: Washington DC, 2009.
4. *Handbook of Batteries*, 3rd ed.; McGraw-Hill: New York, 2002.
5. Stura, E.; Nicolini, C. New Nanomaterials for Light Weight Lithium Batteries. *Anal. Chim. Acta* **2006**, *568*, 57–64.
6. Chan, C. K.; Zhang, X. F.; Cui, Y. High Capacity Li Ion Battery Anodes Using Ge Nanowires. *Nano Lett.* **2008**, *8*, 307–309.
7. Chan, C. K.; Peng, H.; Liu, G.; McIlwrath, K.; Zhang, X. F.; Huggins, R. A.; Cui, Y. High-Performance Lithium Battery Anodes Using Silicon Nanowire. *Nat. Nanotechnol.* **2008**, 3.
8. Chen, W. X.; Lee, J. Y.; Liu, Z. The Nanocomposites of Carbon Nanotubes with Sb and SnSb0.5 as Li-Ion Battery Anodes. *Carbon* **2003**, *41*, 959–966.

9. Eom, J. Y.; Kwon, H. S.; Liu, J.; Zhou, O. Lithium Insertion into Purified and Etched Multi-walled Carbon Nanotubes Synthesized on Supported Catalysts by Thermal CVD. *Carbon* **2004**, *42*, 2589–2596.
10. Frackowiak, E.; Beguin, F. Electrochemical Storage of Energy in Carbon Nanotubes and Nanostructured Carbons. *Carbon* **2002**, *40*, 1775–1787.
11. Frackowiak, E.; Gaurier, S.; Gaucher, H.; Bonnamy, S.; Beguin, F. Electrochemical Storage of Lithium Multiwalled Carbon Nanotubes. *Carbon* **1999**, *37*, 61–69.
12. Guo, Z. P.; Zhao, Z. W.; Liu, H. K.; Dou, S. X. Electrochemical Lithiation and De-lithiation of MWNT-Sn/SnNi Nanocomposites. *Carbon* **2005**, *43*, 1392–1399.
13. Lin, K.; Xu, Y.; He, G.; Wang, X. The Kinetic and Thermodynamic Analysis of Li Ion in Multi-walled Carbon Nanotubes. *Mater. Chem. Phys.* **2006**, *99*, 190–196.
14. Maurin, G.; Bousquet, C.; Henn, F.; Bernier, P.; Almairac, R.; Simon, B. Electrochemical Intercalation of Lithium into Multiwall Carbon Nanotubes. *Chem. Phys. Lett.* **1999**, *312*, 14–18.
15. Maurin, G.; Henn, F. Electrochemical Insertion of Lithium in Carbon Nanotubes. *J. Nanosci. Nanotechnol.* **2004**, *2*, 773–792.
16. Maurin, G.; Henn, F.; Simon, B.; Colomer, J. F.; Nagy, J. B. Lithium Doping of Multiwalled Carbon Nanotubes Produced by Catalytic Decomposition. *Nano Lett.* **2001**, *1*, 75–79.
17. Mukhopadhyay, I.; Hoshino, N.; Kawasaki, S.; Okino, F.; Hsu, W. K.; Touhara, H. Electrochemical Li Insertion in B-Doped Multiwall Carbon Nanotubes. *J. Electrochem. Soc.* **2002**, *149*, A39–A44.
18. Shin, H. C.; Liu, M.; Sadanadan, B.; Rao, A. M. Electrochemical Insertion of Lithium into Multi-walled Carbon Nanotubes Prepared by Catalytic Decomposition. *J. Power Sources* **2002**, *112*, 216–221.
19. Yang, S.; Song, H.; Chen, X.; Okotrub, A. V.; Bulusheva, L. G. Electrochemical Performance of Arc-Produced Carbon Nanotubes as Anode Material for Lithium-Ion Batteries. *Electrochim. Acta* **2007**, *52*, 5286–5293.
20. Yang, Z.; Wu, H. Electrochemical Intercalation of Lithium into Carbon Nanotubes. *Solid State Ionics* **2001**, *143*, 173–180.
21. Yang, Z. H.; Zhou, Y. H.; Sang, S. B.; Feng, Y.; Wu, H. Q. Lithium Insertion into Multi-walled Raw Carbon Nanotubes Pre-doped with Lithium. *Mater. Chem. Phys.* **2005**, *89*, 295–299.
22. Zhao, J.; Gao, Q. Y.; Gu, C.; Yang, Y. Preparation of Multi-walled Carbon Nanotube Array Electrodes and Its Electrochemical Intercalation Behavior of Li Ions. *Chem. Phys. Lett.* **2002**, *358*, 77–82.
23. Nishidate, K.; Hasegawa, M. Energetics of Lithium Ion Adsorption on Defective Carbon Nanotubes. *Phys. Rev. B* **2005**, *71*, 245418.
24. Zhao, J.; Buldum, A.; Han, J.; Lu, J. P. First-Principles Study of Li-Intercalated Carbon Nanotube Ropes. *Phys. Rev. Lett.* **2000**, *85*, 1706.
25. Raffaelle, R. P.; Landi, B. J.; Harris, J. D.; Bailey, S. G.; Hepp, A. F. Carbon Nanotubes for Power Applications. *Mater. Sci. Eng., B* **2005**, *116*, 233–243.
26. Landi, B. J.; Ganter, M. J.; Cress, C. D.; DiLeo, R. A.; Raffaelle, R. P. Carbon Nanotubes for Lithium Ion Batteries. *Energy Environ. Sci.* **2009**, *2*, 638–654.
27. Landi, B. J.; Ganter, M. J.; Schauerman, C. M.; Cress, C. D.; Raffaelle, R. P. Lithium Ion Capacity of Single Wall Carbon Nanotube Paper Electrodes. *J. Phys. Chem. C* **2008**, *112*, 7509–7515.
28. Landi, B. J.; Ganter, M. J.; Schauerman, C. M.; DiLeo, R. A.; Cress, C. D.; Raffaelle, R. P. In *Single Wall Carbon Nanotube-$LiCoO_2$ Lithium Ion Batteries*; Material Research Society Symposium: Boston, MA, 2009.
29. Landi, B. J.; Cress, C. D.; Raffaelle, R. P. High Energy Density Lithium-Ion Batteries with Carbon Nanotube Anodes. *J. Mater. Res.* **2010**, *25*, 1636–1644.
30. Claye, A. S.; Fischer, J. E.; Huffman, C. B.; Rinzler, A. G.; Smalley, R. E. Solid-State Electrochemistry of the Li Single Wall Carbon Nanotube System. *J. Electrochem. Soc.* **2000**, *147*, 2845–2852.
31. Mukhopadhyay, I.; Kawasaki, S.; Okino, F.; Govindaraj, A.; Rao, C. N. R.; Touhara, H. Electrochemical Li Insertion into Single-Wall Carbon Nanotubes Prepared by Graphite Arc-Discharge Method. *Physica B* **2002**, *323*, 130–132.
32. Ng, S. H.; Wang, J.; Guo, Z. P.; Chen, J.; Wang, G. X.; Liu, H. K. Single Wall Carbon Nanotube Paper as Anode for Lithium-Ion Battery. *Electrochim. Acta* **2005**, *51*, 23–28.
33. Eom, J. Y.; Park, J.-W.; Kwon, H. S.; Rajendran, S. Electrochemical Insertion of Lithium into Multiwalled Carbon Nanotube/Silicon Composites Produced by Ballmilling. *J. Electrochem. Soc.* **2006**, *153*, A1678–A1684.
34. Gao, B.; Kleinhammes, A.; Tang, X. P.; Bower, C.; Fleming, L.; Wu, Y.; Zhou, O. Electrochemical Intercalation of Single-Walled Carbon Nanotubes with Lithium. *Chem. Phys. Lett.* **1999**, *307*, 153–157.
35. Chan, C. K.; Zhang, X. F.; Cui, Y. High Capacity Li Ion Battery Anodes Using Ge Nanowires. *Nano Lett.* **2008**, *8*, 307–309.
36. Meduri, P.; Pendyala, C.; Kumar, V.; Sumanasekera, G. U.; Sunkara, M. K. Hybrid Tin Oxide Nanowires as Stable and High Capacity Anodes for Li-Ion Batteries. *Nano Lett.* **2009**, *9*, 612–616.
37. Kim, T.; Mo, Y. H.; Nahm, K. S.; Oh, S. M. CNTs as a Buffer Layer in Silicon/CNTs Composite Electrodes for Lithium Secondary Batteries. *J. Power Sources* **2006**, *162*, 1275–1281.
38. Zhang, Y.; Zhang, X. G.; Zhang, H. L.; Zhao, Z. G.; Li, F.; Liu, C.; Cheng, H.-M. Composite Anode Material of Silicon/Graphite/Carbon Nanotubes for Li-Ion Batteries. *Electrochim. Acta* **2006**, *51*, 4994–5000.
39. Chen, Y.-J.; Zhu, C.-L.; Xue, X.-Y.; Shi, X.-L.; Cao, M.-S. High Capacity and Excellent Cycling Stability of Single-Walled Carbon Nanotube/SnO_2 Core−Shell Structures as Li-Insertion Materials. *Appl. Phys. Lett.* **2008**, *92*, 223101.
40. Chen, G.; Wang, Z.; Xia, D. One-Pot Synthesis of Carbon Nanotube-SnO_2-Au Coaxial Nanocable for Lithium Ion Batteries with High Rate Capability. *Chem. Mater.* **2008**, *20*, 6951–6956.
41. Cui, L.-F.; Hu, L.; Choi, J. W.; Cui, Y. Light-Weight Free-Standing Carbon Nanotube−Silicon Films for Anodes of Lithium Ion Batteries. *ACS Nano* **2010**, *4*, 3671−3678.
42. DiLeo, R. A.; Ganter, M. J.; Landi, B. J.; Raffaelle, R. P. Germanium-Single Wall Carbon Nanotube Anodes for Lithium Ion Batteries. *J. Mater. Res.* **2010**, *25*, 1441–1446.
43. Andriotis, A. N.; Menon, M.; Froudakis, G. E. Various Bonding Configurations of Transition-Metal Atoms on Carbon Nantubes: Their Effect on Contact Resistance. *Appl. Phys. Lett.* **2000**, *76*, 3890–3892.
44. Dag, S.; Durgun, E.; Ciraci, S. High-Conducting Magnetic Nanowires Obtained from Uniform Titanium-Covered Carbon Nanotubes. *Phys. Rev. B* **2004**, 69.
45. He, Y.; Zhang, J.; Hou, S.; Wang, Y.; Yu, Z. Schottky Barrier Formation at Metal Electrodes and Semiconducting Carbon Nanotubes. *Appl. Phys. Lett.* **2009**, 94.
46. He, Y.; Zhang, J.; Wang, Y.; Yu, Z. Coating Geometries of Metals on Single-Walled Carbon Nanotubes. *Appl. Phys. Lett.* **2010**, 96.
47. Leonard, F.; Talin, A. A. Size-Dependent Effects on Electrical Contacts to Nanotubes and Nanowires. *Phys. Rev. Lett.* **2006**, 97.
48. Matsuda, Y.; Deng, W.-Q.; Goddard, W. A., III. Contact Resistance Properties between Nanotubes and Various Metals from Quantum Mechanics. *J. Phys. Chem. C* **2007**, *111*, 11113–11116.
49. Vitale, V.; Curioni, A.; Andreoni, W. Metal−Carbon Nanotube Contacts: The Link between Schottky Barrier and Chemical Bonding. *J. Am. Chem. Soc.* **2008**, *130*, 5848–5849.
50. Yang, C.-K.; Zhao, J.; Lu, J. P. Binding Energies and Electronic Structures of Adsorbed Titanium Chains on Carbon Nanotubes. *Phys. Rev. B* **2002**, *66*, 041403.

51. Zhang, Y.; Li, J.; Zhou, L.; Xiang, S. A Theoretical Study on the Chemical Bonding of 3D-Transition-Metal Carbides. *Solid State Commun.* **2002**, *121*, 411–416.
52. Chen, C.; Liu, L.; Lu, Y.; Kong, E. S.-W.; Zhang, Y.; Sheng, X.; Ding, H. A Method for Creating Reliable and Low-Resistance Contacts between Carbon Nanotubes and Microelectrodes. *Carbon* **2007**, *45*, 436–442.
53. Lim, S. C.; Jang, J. H.; Bae, D. J.; Han, G. H.; Lee, S.; Yeo, I.-S.; Lee, Y. H. Contact Resistance between Metal and Carbon Nanotube Interconnects: Effect of Work Function and Wettability. *Appl. Phys. Lett.* **2009**, 95.
54. Tseng, Y.-C.; Bokor, J. Characterization of the Junction Capacitance of Metal-Semiconductor Carbon Nantoube Schottky Contacts. *Appl. Phys. Lett.* **2010**, 96.
55. Peng, N.; Li, H.; Zhang, Q. Nanoscale Contacts between Carbon Nanotubes and Metallic Pads. *ACS Nano* **2009**, *3*, 4117–4121.
56. Jackson, R.; Graham, S. Specific Contact Resistance at Metal/Carbon Nanotube Interfaces. *Appl. Phys. Lett.* **2009**, 94.
57. Chen, C.; Yan, L.; Kong, E. S.-W.; Zhang, Y. Ultrasonic Nanowelding of Carbon Nanotubes to Metal Electrodes. *Nanotechnology* **2006**, *17*, 2192–2197.
58. Tran, I. C.; Felix, R.; Bar, M.; Weinhardt, L.; Zhang, Y.; Heske, C. Oxidation of Titanium-Decorated Single-Walled Carbon Nanotubes and Subsequent Reduction by Lithium. *J. Am. Chem. Soc.* **2010**, *132*, 5789–5792.
59. Qin, Y.; Hu, M. Characterization and Field Emission Characteristics of Carbon Nanotubes Modified by Titanium Carbide. *Appl. Surf. Sci.* **2008**, *254*, 3313–3317.
60. Uh, H. S.; Park, S.; Kim, B. Enhanced Field Emission Properties Form Titanium-Coated Carbon Nanotubes. *Diamond Relat. Mater.* **2010**, *19*, 586–589.
61. Nosho, Y.; Ohno, Y.; Kishimoto, S.; Mizutani, T. Relation between Conduction Property and Work Function of Contact Metal in Carbon Nanotube Field-Effect Transistors. *Nanotechnology* **2006**, *17*, 3412–3415.
62. Luo, W.; Ravichandran, K.; Windl, W.; Fonseca, L. R. C. Ab-Initio Modeling of Contact Structure Formation of Carbon Nanotubes with Different Metals and Its Effect on Electron Transport. *Materials Research Society*, 2008.
63. Perello, D. J.; ChuLim, S.; Chae, S. J.; Lee, I.; Kim, M. J.; Lee, Y. H.; Yun, M. Anomalous Schottky Barriers and Contact Band-to-Band Tunneling in Carbon Nanotube Transistors. *ACS Nano* **2010**, *4*, 3103–3108.
64. Chen, Z.; Appenzeller, J.; Knoch, J.; Lin, Y.-m.; Avouris, P. The Role of Metal−Nanotube Contact in the Performance of Carbon Nanotube Field-Effect Transistors. *Nano Lett.* **2005**, *5*, 1497–1502.
65. Lan, C.; Srisungsitthisunti, P.; Amama, P. B.; Fisher, T. S.; Xu, X.; Reifenberger, R. G. Measurement of Metal/Carbon Nanotube Contact Resistance by Adjusting Contact Length Using Laser Ablation. *Nanotechnology* **2008**, 19.
66. Felten, A.; Martinez, I. S.; Ke, X.; Tendeloo, G. V.; Ghijsen, J.; Pireaux, J.-J.; Drube, W.; Bittencourt, C.; Ewels, C. P. The Interface between Titanium and Carbon Nanotubes. *Chem. Phys. Chem.* **2009**, *10*, 1799–1804.
67. Zhang, Y.; Dai, H. Formation of Metal Nanowires on Suspended Single-Walled Carbon Nanotubes. *Appl. Phys. Lett.* **2000**, *77*, 3015–3017.
68. Zhang, Y.; Franklin, N. W.; Chen, R. J.; Dai, H. Metal Coating on Suspended Carbon Nanotubes and Its Implication to Metal−Tube Interaction. *Chem. Phys. Lett.* **2000**, *331*, 35–41.
69. Durgun, E.; Dag, S.; Bagci, V. M. K.; Gulseren, O.; Yildirim, T.; Ciraci, S. Systematic Study of Adsorption of Single Atoms on a Carbon Nanotube. *Phys. Rev. B* **2003**, 67.
70. Liu, Z.; Ci, L.; Bajwa, N.; Ajayan, P. M.; Lu, J.-Q. Benchmarking of Metal-to-Carbon Nanotube Side Contact Resistance. *IEEE International Interconnect Technology Conference*, 2008; pp 144−146.
71. Park, M.; Cola, B. A.; Siegmund, T.; Xu, J.; Maschmann, M. R.; Fisher, T. S.; Kim, H. Effects of a Carbon Nanotube Layer on Electrical Contact Resistance between Copper Substrates. *Nanotechnology* **2006**, *17*, 2294–2303.
72. Yaglioglu, O.; Hart, A. J.; Martens, R.; Slocum, A. H. Method of Characterizing Electrical Contact Properties of Carbon Nanotube Coated Surfaces. *Rev. Sci. Instrum.* **2006**, 77.
73. Yunus, E. M.; Spearing, S. M.; McBride, J. W. The Relationship between Contact Resistance and Contact Force on Au Coated Carbon Nanotube Surfaces. The 53rd IEEE Holm Conference on Electrical Contacts, 2007; pp 167−174.
74. Mukhopadhyay, I.; Touhara, H. Different Methods of Preparing Electrode from Single-Wall Carbon Nanotubes and Their Effect on the Li Ion Insertion Process. *J. Solid State Electrochem.* **2008**, *12*, 715–720.
75. Wang, J.; Polleux, J.; Lim, J.; Dunn, B. Pseudocapacitive Contributions to Electrochemical Energy Storage in TiO_2 (Anatase) Nanoparticles. *J. Phys. Chem. C* **2007**, *111*, 14925–14931.
76. Xu, J.; Jia, C.; Cao, B.; Zhang, W. F. Electrochemical Properties of Anatase TiO_2 Nanotubes as an Anode Material for Lithium-Ion Batteries. *Electrochim. Acta* **2007**, *52*, 8044–8047.
77. Kishiyama, C.; Nagata, M.; Piao, T.; Dodd, J.; Lam, P. K.; Tsukamoto, H. Improvement of Deep Discharge Capability for Lithium Ion Batteries. *Proc. Electrochem. Soc.* **2004**, *28*, 352–359.
78. Chung, S.-Y.; Bloking, J. T.; Chiang, Y.-M. Electronically Conductive Phospho-olivines as Lithium Storage Electrodes. *Nat. Mater.* **2002**, *1*, 123–128.
79. Nechev, K. SAFT's Very High Power Li-Ion Technology. 3rd Annual International Conference Lithium Mobile Power; The Knowledge Foundation Press: San Diego, CA, 2007.
80. Joachin, H.; Kaun, T. D.; Zaghib, K.; Prakash, J. Electrochemical and Thermal Studies of Carbon-Coated $LiFePO_4$ Cathode. *J. Electrochem. Soc.* **2009**, *156*, A401–A406.
81. Liu, Y. *Ab Initio* Study of Ti-Contacted Single-Walled Carbon Nanotube. *Phys. Rev. B* **2003**, 68.
82. Lim, S. C.; Jang, J. H.; Bae, D. J.; Han, G. H.; Lee, S.; Yeo, I.-S.; Lee, Y. H. Contact Resistance between Metal and Carbon Nanotube Interconnects: Effect of Work Function and Wettability. *Appl. Phys. Lett.* **2009**, 95.
83. *CRC Handbook of Chemistry and Physics*, 77th ed.; CRC Press: New York, 1996.
84. Walton, S. G.; Tucek, J. C.; Champion, R. L.; Wang, Y. Low Energy, Ion-Induced Electron and Ion Emission from Stainless Steel: The Effect of Oxygen Coverage and the Implications for Discharge Modeling. *J. Appl. Phys.* **1999**, *85*, 1832–1837.
85. Shiraishi, M.; Ata, M. Work Function of Carbon Nanotubes. *Carbon* **2001**, *39*, 1913–1917.
86. Ouyang, M.; Huang, J.-L.; Cheung, C. L.; Lieber, C. M. Energy Gaps in "Metallic" Single-Walled Carbon Nanotubes. *Science* **2001**, *292*, 702–705.
87. Strano, M. S. Probing Chiral Selective Reactions Using a Revised Kataura Plot for the Interpretation of Single-Walled Carbon Nanotube Spectroscopy. *J. Am. Chem. Soc.* **2003**, *125*, 16148–16153.
88. Saito, R.; Dresselhaus, G.; Dresselhaus, M. S. Trigonal Warping Effect of Carbon Nanotubes. *Phys. Rev. B* **2000**, *61*, 2981–2990.
89. McDonald, T. J.; Svedruzic, D.; Kim, Y.-H.; Blackburn, J. L.; Zhang, S. B.; Tang, P. W.; Heben, M. J. Wiring up Hydrogenase with Single-Walled Carbon Nanotubes. *Nano Lett.* **2007**, *7*, 3528–3534.
90. Dukovic, G.; Wang, F.; Song, D.; Sfeir, M. Y.; Heinz, T. F.; Brus, L. E. Structural Dependence of Excitonic Optical Transitions and Band-Gap Energies in Carbon Nanotubes. *Nano Lett.* **2005**, *5*, 2314–2318.
91. Landi, B. J.; Ruf, H. J.; Evans, C. M.; Cress, C. D.; Raffaelle, R. P. Purity Assessment of Single-Wall Carbon Nanotubes, Using Optical Absorption Spectroscopy. *J. Phys. Chem. B* **2005**, *109*, 9952–9965.
92. Santerre, F.; Khakani, M. A. E.; Chaker, M.; Dodelet, J. P. Properties of TiC Thin Films Grown by Pulsed Laser Deposition. *Appl. Surf. Sci.* **1999**, *148*, 24–33.